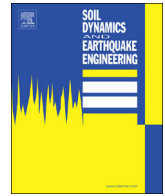




ELSEVIER

Contents lists available at ScienceDirect

## Soil Dynamics and Earthquake Engineering

journal homepage: [www.elsevier.com/locate/soildyn](http://www.elsevier.com/locate/soildyn)

## Pre-shaking effects on volumetric strain and cyclic strength of sand and comparison to unsaturated soils

Mitsu Okamura\*, Fred Nelson, Shota Watanabe

Graduate School of Science and Engineering – Ehime University, Japan

## ARTICLE INFO

**Keywords:**  
Liquefaction  
Sand  
Aging effect  
Pre-shaking  
Centrifuge test  
Triaxial test

## ABSTRACT

Repeated small shaking events due to earthquakes significantly enhance liquefaction resistance of soils. Analyses of liquefaction case histories show that aged soils in seismically active zones tend to be less vulnerable to liquefaction despite having similar index parameters—such as standard penetration test N-values and shear wave velocities—as young soils. Significant efforts have been devoted to better understand the effects of the cyclic pre-shearing on liquefaction resistance and it was found that this effect depends on the number of cycles and cyclic stress ratio. However, none of these parameters quantify the improvement of liquefaction resistance due to pre-shaking. This study investigates the pre-shearing effects on liquefaction resistance through laboratory tests and centrifuge tests. An attempt was made to explain the effects quantitatively with a single index parameter of the volumetric strain caused by pre-shearing. It was confirmed from triaxial tests that the liquefaction resistance of pre-sheared sand uniquely increased with increasing volumetric strain regardless of the cyclic shear stress ratio and the number of cycles during the pre-shearing. To examine the pre-shaking effects on the liquefaction strength of sand under a level ground condition, centrifuge tests were conducted in this study. Sand models were subjected to small shaking events repeatedly, which were weak enough not to cause liquefaction. It was observed that changes in the index parameters of the models, including soil density (volumetric strain), shear wave velocity, and horizontal earth pressure during the pre-shaking events were very small. At the end of the test, the sand was subjected to a strong shaking event because models that had gone through pre-shaking need larger shaking acceleration to liquefy. Liquefaction resistance was derived from acceleration records with the aid of the cumulative damage theory. The relationship between liquefaction resistance ratio and volumetric strain that occurred in the pre-shaking events coincides with the relationship obtained from the triaxial tests. After the extensive liquefaction event, all index parameters except soil density— $K_o$ ,  $V_s$ , liquefaction resistance—tended to return to their original values (before the pre-shaking).

### 1. Introduction

The resistance to liquefaction of sandy soils that have been resting for many years is greater than that of recently deposited soils. This aging effect on liquefaction resistance may be explained by two mechanisms. One is the improved interlocking of sand grains developed after deposition, which is associated with their extended time under static pressure and being subjected to repeated earthquake shakings. The other mechanism is the long period of sustained static load [17] that is probably associated with such chemical reactions as dissolution of minerals and precipitation at soil grain surface, which develop bonding between soil particles. The focus of this paper is on the first mechanism.

It was pointed out that repeated small shakings due to earthquakes significantly enhance soil liquefaction resistance. Analyses of liquefaction case histories showed that older soils in seismically active zones

tend to be less vulnerable to liquefaction although their index parameters—such as standard penetration test N-values and shear wave velocities—were very similar [4,11]. Moreover, these facts are supported by many laboratory tests [7,9,12,19,20]. In view of these, significant efforts in laboratory testing were devoted to better understand the effects of cyclic pre-shearing on liquefaction resistance. The test results consistently indicated that the liquefaction resistance increased with the number of cycles and cyclic stress ratio provided that the shear strain during pre-shearing was small. However, none of these parameters quantify the improvement of the liquefaction resistance due to pre-shaking.

The effects of seismic-shaking history of soils on liquefaction triggering were investigated through a carefully designed centrifuge test [5,6]. In the test, a uniform, silty sand deposit was subjected to multiple shaking events with horizontal base accelerations, most of which were short to liquefy the sand. They concluded that there was a significant

\* Corresponding author.

<https://doi.org/10.1016/j.soildyn.2018.04.046>

Received 12 September 2017; Received in revised form 1 April 2018; Accepted 25 April 2018

0267-7261/ © 2018 The Authors. Published by Elsevier Ltd. This is an open access article under the CC BY-NC-ND license (<http://creativecommons.org/licenses/by-nc-nd/4.0/>).

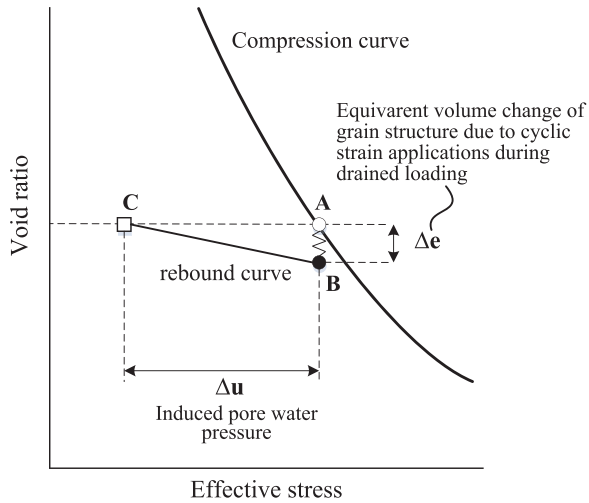


Fig. 1. Contraction by cyclic shearing and generation of pore pressure (after [19]).

increase in the resistance of the sand deposit to excess pore pressure generation because it was exposed to an increasing number of shaking events although the change in relative density was small.

It was also recognized that once sand experiences large strains, including extensive liquefaction, its liquefaction resistance decreases, rather than increases, indicating that the beneficial effects of pre-shakings by previous earthquakes are lost. This phenomenon was confirmed by several field evidences [2], laboratory tests [7,9,23] as well as the centrifuge test [5,6].

This study aims at further investigating the pre-shaking effects on liquefaction resistance through laboratory and centrifuge tests. An attempt is made to explain the effect quantitatively by a single index of the volumetric strain caused by the pre-shaking.

2. Significance of volumetric strain

The basic mechanics of volumetric contraction and pore pressure generation in the undrained cyclic shearing was conceptually demonstrated by [19]. Soil grain structure tends to contract when subjected to cyclic shearing—indicated as from points A to B in Fig. 1. If the undrained condition is imposed, volume contraction is shifted to pore pressure generation and reduction in effective stress. As a result, the soil grain structure rebounds to the extent required to keep the volume constant—indicated as from points B to C in the rebound line. Cyclic shearing induced contraction, whereas soil structure rebound determined the magnitude of excess pore pressure generation in the soil.

Finn [8] found a relationship between volumetric contraction and generated excess pore pressure based on cyclic shear tests. For medium-dense clean sand, excess pore pressure ratio uniquely correlated with the volumetric strain and a volumetric strain (in the order of 1%) was needed to reach a condition close to liquefaction (excess pore pressure ratio higher than 90%).

Fig. 2 demonstrates conceptually the evolution of volumetric strain of sand with the number of cycles in the drained condition. From the figure, it can be observed that the increase of the volumetric strain slows down with increasing number of cycles. However, when the same cyclic shearing is conducted under the undrained condition, sand liquefies in the  $N_{L1}$ th cycle which corresponds to the volumetric strain needed to reach the liquefaction condition,  $\epsilon_{vL}$ . Therefore, for pre-shaking to cause a volumetric strain of  $\epsilon_{ps}$ , the sand must have used up its ability of contraction to the extent and it will need  $(N_{L2} - N_{ps})$  cycles to yield further volumetric strain,  $\epsilon_{vL}$ , to liquefy under undrained cyclic shearing. Because of the convex shape of the curve shown in the figure, the number of cycles  $(N_{L2} - N_{ps})$  is larger than  $N_{L1}$  and their difference

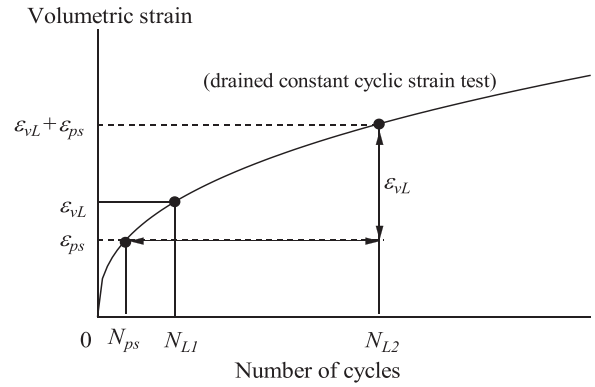


Fig. 2. Schematic illustration of evolution of volumetric strain due to drained cyclic shearing.

may be recognized as the beneficial effect—i.e., the pre-shearing effect—on the liquefaction resistance.

It is of interest to note that increases in the liquefaction resistance due to imperfect saturation of soils, membrane penetration, and partial drainage during shearing are also explained in terms of the volumetric strain. It is known that unsaturated soils exhibit higher liquefaction resistance than fully saturated soils. The underlying mechanism that enhance the liquefaction resistance of unsaturated sand is that air in a partially saturated sand mass absorbs generated excess pore pressures by reducing its volume [16]. The soil mass, or the soil grain structure, needs to yield a volumetric strain,  $(\epsilon_v^* + \epsilon_{vL})$ —where  $\epsilon_v^*$  denotes the soil volumetric strain due to compression of air contained in the soil mass—to reach the liquefaction condition. Accordingly, the number of cycles are larger than  $N_{L1}$ . In relation to this, Okamura and Soga [16] found a unique relationship between  $\epsilon_v^*$  and liquefaction resistance ratio (LRR), which is the ratio of the cyclic shear stress ratio to that of the soil at a fully saturated condition, as shown in Fig. 3. In this regard, volumetric strain caused by partial drainage during shearing is considered to play the same role as  $\epsilon_v^*$  for unsaturated soils.

In the next section, the pre-shearing effects on liquefaction resistance are investigated through a series of cyclic triaxial tests on clean sand with and without pre-shearing histories from the viewpoint of volumetric strain caused during pre-shearing.

3. Triaxial test

3.1. Test procedures and conditions

The material used in the test was Toyoura sand with a specific gravity of 2.64, and minimum and maximum void ratios of  $e_{min} = 0.609$  and  $e_{max} = 0.973$ , respectively [15]. A total of 27 tests was

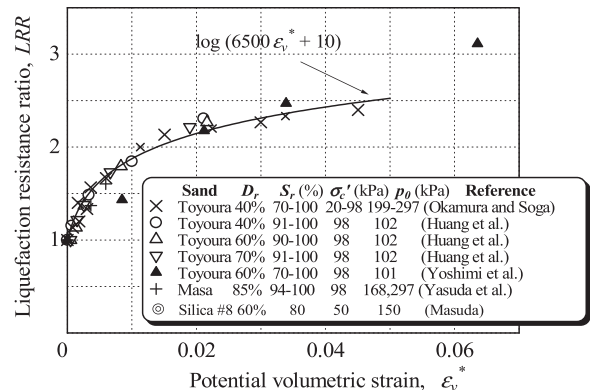


Fig. 3. Relationship between potential volumetric strain and liquefaction resistance of partially saturated sand (after Okamura and Soga [16]).

**Table 1**  
Triaxial test conditions.

Relative density, $D_r$ (%) <sup>a</sup>	Pre-shearing		Liquefaction test	
	Target vol. strain, $\epsilon_v$ (%)	Cyclic stress ratio, $CSR_{ps}$ <sup>b</sup>	Approx. no. of cycles $N_{ps}$ <sup>b</sup>	Cyclic stress ratio, $CSR_L$ <sup>c</sup>
40–45	0	–	–	0.12, 0.14, 0.18, 0.19
39–45	0.1	0.05	650	0.16, 0.17, 0.18, 0.19
		0.10	320	
		0.14	21	
		0.15	11	
39–44	0.33	0.10	490	0.18, 0.21, 0.22
		0.15	380	
		0.20	30	
		0.25	10	
		0.28	2	
41–46	0.77	0.25	200	0.21, 0.22, 0.23, 0.27, 0.28, 0.29
		0.27	80	

<sup>a</sup> Relative density of specimens before pre-sharing.

<sup>b</sup> Cyclic stress ratio and number of cycles in pre-shearing.

<sup>c</sup> Cyclic stress ratio in liquefaction test.

carried out, where all of the specimens were prepared by pouring dry sand from a funnel through air to attain a target relative density of  $D_r = 45\%$ . All specimens were 50 mm in diameter and 100 mm in height. After saturating the specimens and confirming that the B value is higher than 0.95, the specimens were consolidated at an isotropic effective confining pressure of  $\sigma'_c = 50$  kPa, followed by pre-shearing in the drained condition with a constant cyclic stress ratio,  $CSR_{ps}$ , and a frequency of 0.01 Hz. The frequency was selected to be low enough so as not to build up any excess pore pressure. The pre-shearing was continued until the target volume change was achieved. The four target volumetric strains in the pre-shearing set in this study are  $\epsilon_v = 0\%$  (without pre-shearing), 0.1%, 0.33%, and 0.77%. It should be noted that several different combinations of  $CSR_{ps}$  and number of cycles of the pre-shearing,  $N_{ps}$ , were tested for each target volumetric strain. Following pre-shearing, undrained cyclic shear tests were conducted with constant cyclic stress ratio,  $CSR_L$ . The test conditions are summarized in Table 1.

3.2. Test results

Fig. 4 shows typical time histories obtained during pre-shearing. It can be observed that volumetric contraction increased with the number of cycles, and that contraction rate was initially high and then slowed down as the number of cycles increased until it attained the target

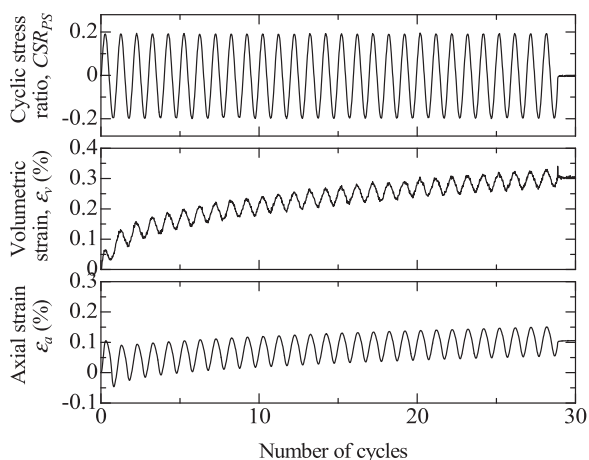


Fig. 4. Evolution of axial and volumetric strain during pre-shearing.

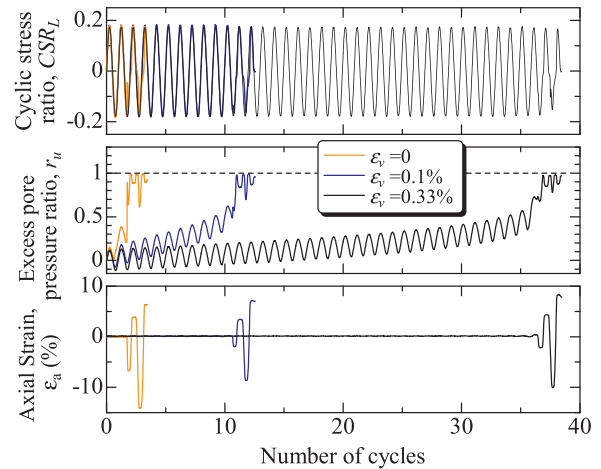


Fig. 5. Responses to undrained cyclic shearing of specimens with and without pre-shaking ( $\epsilon_v = 0, 0.1\%$  and  $0.33\%$ ).

volumetric strain of  $\epsilon_v = 0.33\%$ . After pre-shearing, specimens were subjected to cyclic shearing in the undrained condition. The typical responses of the specimens are shown in Fig. 5, along with those of specimens with  $\epsilon_v = 0.33\%$  and without any pre-shearing history (i.e.,  $\epsilon_v = 0\%$ ). For the same cyclic stress ratio ( $CSR_L$ ), the specimen with pre-shearing history developed excess pore pressure at a much lower rate than that without pre-shearing. On the other hand, the deformations of the specimens after liquefaction, which is associated with ground deformation and earthquake damage to structures, are quite similar. Axial strain amplitudes developed with the number of cycles in a similar manner. It can be said that the pre-shearing history has a significant effect on liquefaction triggering but this is not the case for the deformation characteristics after liquefaction condition is reached.

Fig. 6 depicts the relationship between cyclic stress ratio in the liquefaction tests,  $CSR_L$ , and the number of the cycles to attain double amplitude axial strain  $DA = 5\%$  for all tests. It shows that  $CSR_L$  increased with an increase in  $\epsilon_v$ . Moreover, a slight volumetric strain of 0.77%, which corresponds to an increase in the relative density of only 3.7%, almost doubled the  $CSR_L$  of the medium dense sand. One may consider that the increase in relative density due to the pre-shearing is responsible for the significant increase in  $CSR_L$ ; however, change of a few percentage points in relative density of medium dense sand alone does not practically affect the liquefaction resistance. Although there is a good correlation between relative density and liquefaction resistance

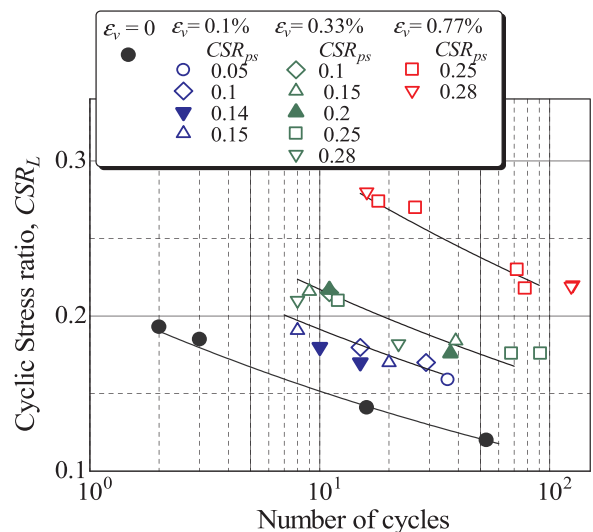


Fig. 6. Liquefaction resistance curves.

of re-constituted sand, relative density is not a good index of liquefaction resistance for sand with pre-shearing history.

It should also be mentioned that the plots in the figure for the same target volumetric strain lie almost along the same line even though they were subjected to pre-shearing with different combinations of  $CSR_{ps}$  and number of cycles,  $N_{ps}$ .

Finn et al. [7] stated that the beneficial effect of pre-shearing on liquefaction resistance became less as shear strain amplitude during pre-shaking increased. It is presumed that a small shear strain amplitude of pre-shearing improves soil grain contacts and enhances the stability of soil skeleton, consequently resulting in higher liquefaction resistance. On the contrary, a larger shear strain amplitude, degrades the stability of soil skeleton. According to Finn et al., the threshold shear strain amplitude above which the beneficial effect ceases was approximately 0.5%. In the present study, shear strain amplitude in the pre-shearing is lower than 0.24% and degradation in the liquefaction resistance is not observed from any of the tests. More details on the above are provided elsewhere.

### 3.3. Effects of volumetric strain due to pre-shearing

The test results described above suggest that volumetric strain is the main parameter that governs the improvement of liquefaction resistance due to pre-shearing. The liquefaction resistance increased with increasing volumetric strain regardless of  $CSR_{ps}$  and  $N_{ps}$ , as shown in Fig. 6.

An increase in liquefaction resistance due to volumetric strain has also been observed in studies on unsaturated sand, membrane penetration, and system compliance. The sand subjected to pre-shearing experienced volumetric strain before undrained cyclic shearing, whereas it is generated during undrained cyclic shearing for unsaturated sand and coarse sand with the membrane penetration effect. Irrespective of whether volumetric strain occurs before or during cyclic shearing, the volumetric strain is considered to have the same effect on liquefaction resistance. This may be explained by the discussion in the preceding section on Fig. 2 that volumetric strain, both due to pre-shearing and imperfect saturation, increases the number of cycles needed to cause liquefaction. It is interesting to compare the effects of all these phenomena on liquefaction resistance. In this study, the liquefaction resistance ratio,  $LRR_{ps}$ , is defined as the liquefaction resistance of sand with pre-shearing history ( $DA = 5\%$ ,  $N = 20$ ) normalized with respect to the liquefaction resistance of sand without pre-shearing, as shown in Fig. 7, together with test results reported by Goto and Towhata [9], Okamura and Soga [16], and Tokimatsu and Nakamura [22]. With regard to the pre-shearing effect, results from this

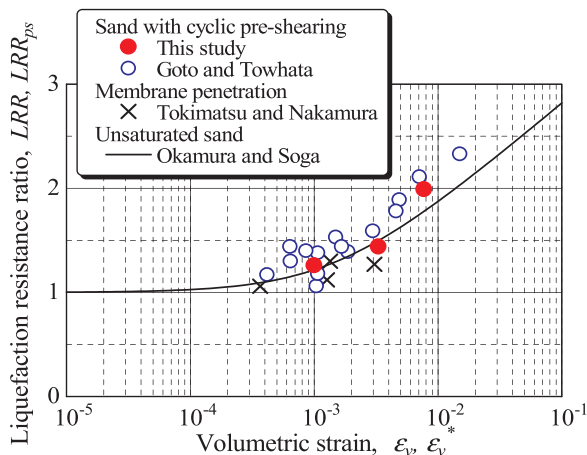


Fig. 7. Relationship between liquefaction resistance ratio and volumetric strain of sand with pre-shearing of unsaturated sand and sand in partial drainage condition.

study, and that of [9], agree quite well even though the soils used and relative density of specimens are different. The test results also agree well with those obtained by Okamura and Soga [16], and Tokimatsu and Nakamura [22].

## 4. Centrifuge test

Centrifuge tests were conducted to examine in detail the effects of pre-shaking effects on the liquefaction strength characteristics of 3 m deep uniform sand deposits. Fully saturated medium-dense sand models were prepared and subjected to multiple shaking events sufficiently weak so as not to liquefy the model. The change in index parameters, including soil density (volumetric strain), shear wave velocity, and horizontal earth pressure were observed. The subsequent motions imparted to the models were sufficiently strong to liquefy the sand.

The three models tested here had the same relative density and were prepared employing the same deposition method of dry pluviation as that used for the triaxial specimen. In addition, two more tests were conducted on models with the same relative density but different initial soil fabric.

### 4.1. Centrifuge model preparation

Toyoura sand deposited at a relative density of  $Dr = 45\%$  was used in all the centrifuge tests presented in this paper. At that density, the permeability of the sand is  $k = 2.5 \times 10^{-4}$  m/s tested at 1 g using water as pore fluid.

A rectangular laminar container was used in all the tests. The box was designed to shake a plane strain geotechnical model in the long direction of the box, and is optimized to accommodate and measure accurately a wide range of cyclic and permanent lateral displacements occurring in the soil model. A side view of the instrumented model in the laminar box is presented in Fig. 8. The box, mostly made of a high strength duralumin alloy and having internal dimensions (width, length, and depth) of 12 cm, 40 cm, and 22 cm, respectively, is comprised of a stack of up to 22 rectangular rings separated by linear roller bearings. A latex rubber membrane, 0.5 mm thick, was used to line the inside of the laminar box to prevent leakage of the contents.

A total of five uniform sand models, each 12 cm deep with a relative density of  $Dr = 45\%$  were tested in this study as listed in Table 2. Two types of sand deposition methods were employed to construct the models. Three models, models 1–3, were prepared by pouring dry sand into the laminar box from a funnel in the same manner as the triaxial testing mentioned previously. A wet tamping method was used for the other two models, models 4 and 5, where the sand with a water content of 10% was compacted at every 1 cm thick 12 times. During model preparation, accelerometers, pore pressure and earth pressure cells, and

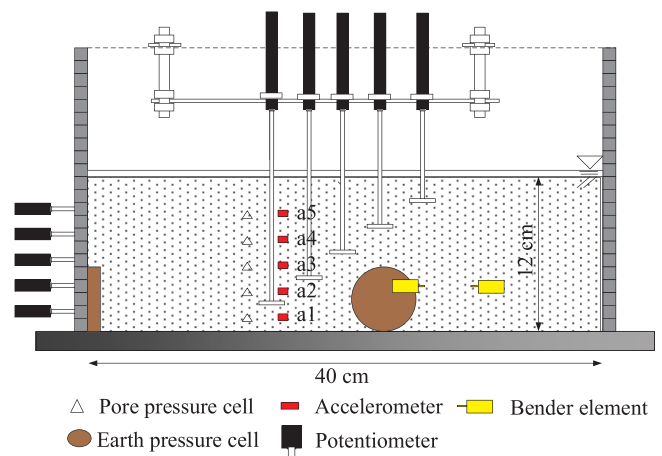


Fig. 8. Centrifuge model setup (in model scale, to-scale drawing).

**Table 2**  
Centrifuge test conditions.

Model #	Degree of saturation, Sr (%)	Relative density		Target and actual vol. strain (%)	No. of pre-shaking events
		Before shaking, Dr <sub>0</sub> (%)	After pre-shaking, Dr (%)		
< sand deposition method: dry pluviation >					
1	99.8	48	–	0	0
2	99.7	49	51	0.33 / 0.36	9
3	99.9	48	52	0.77 / 0.80	17
< sand deposition method: wet tamping >					
4	99.7	49	–	0	0
5	99.7	47	52	0.77 / 1.08	12

potentiometers were installed according to proper orientations and locations.

De-aired fluid was introduced through the top of the model in a vacuum chamber at a pressure of  $-95$  kPa to saturate until the fluid level in the laminar box rose above the surface of the soil. Employing the measurement method proposed by Okamura and Inoue [15], the degree of saturation of the models was in the range of 99.40–99.65%, which became higher in the centrifuge environment with the hydrostatic pore pressure increased 25 times higher.

The model sand deposits utilized in this centrifuge test were saturated with a viscous fluid, which was a mixture of water and hydroxypropyl methylcellulose. This Metolose pore fluid solution was prepared by dissolving 2% Metolose by weight in water to achieve a viscosity of about 50 times the viscosity of water (kinematic viscosity,  $\nu = 50$  cSt). All the centrifuge tests in this study were conducted with a 25 g centrifugal acceleration. The consequence in using the pore fluid with a viscosity  $\nu$  times higher than that of water in the centrifuge tests at 25 g to model the liquefaction of the water-saturated prototype soil in the field is that **the actual prototype permeability** being simulated was  $k_{\text{prototype}} = k/\nu \cdot 25$  (Tan and Scott, [21]).

The purpose of centrifuge testing with a viscous pore fluid is to simulate more closely the undrained condition during shaking. Okamura and Hayashi [14] conducted a series of centrifuge tests on thin sand layers (the prototype depth of liquefiable sand layer was 1.0 m) to investigate the effects of sand permeability on liquefaction triggering acceleration. The input acceleration is necessary to make the sand deposit liquefy, and thus, an apparent liquefaction resistance increased with increasing sand permeability. Partial drainage during shaking is responsible for the observed increase in the apparent liquefaction resistance. Based on their test results, it is estimated that the  $k_{\text{prototype}} = 1.25 \times 10^{-4}$  m/s ( $\nu = 50$  cSt) is low enough to impose the undrained condition to a 3 m deep Toyoura sand deposit. Therefore, the centrifuge models in this study, as listed in Table 2, simulated induced pre-shakings and liquefaction in the field of the same prototype layer (homogeneous deposit of uniform clean sand of  $Dr = 45\%$ ) in the undrained condition.

#### 4.2. Test procedures

The model in the laminar box was set on the centrifuge platform and the centrifuge was gradually brought to 25 g. A series of one dimensional lateral shakings, with the basic shape of acceleration time histories shown in Fig. 9, were imparted along the model long axis using a mechanical shaker. Hereinafter, in this paper, all results and comparisons are presented in prototype units unless specified otherwise.

El-Sekelly et al. [5,6] conducted centrifuge tests on a 6 m prototype medium-dense silty sand deposits to study the effects of pre-shaking on liquefaction resistance. Their testing program was elaborately designed; the base of the model was subjected to a number of shaking events of different accelerations. The researchers observed a significant increase in the resistance of the deposits in generating excess pore water

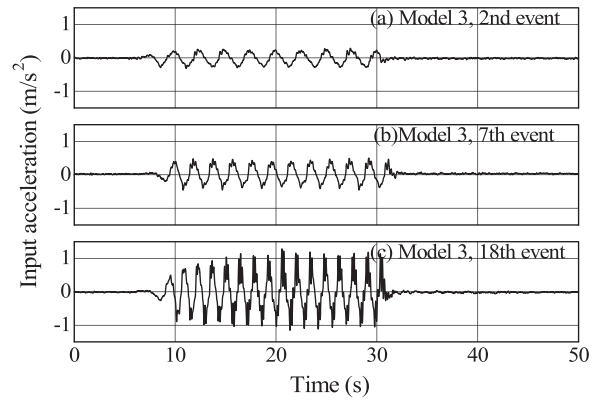


Fig. 9. Typical input acceleration time histories.

pressure as these were exposed to an increasing number of small shaking events.

In the present study, volumetric strain was closely monitored throughout the shaking events. The test conditions are listed in Table 2. For model 1, without pre-shaking, the input acceleration of the first shaking event, which was a destructive one, was as strong as that estimated from the results of the triaxial tests on the sand without pre-shearing. The cyclic stress ratio needed to liquefy the sand in 10 cycles is 0.15 (Fig. 5), which corresponds to an input acceleration amplitude of  $A_0 = 0.45$  m/s<sup>2</sup>. Note that the liquefaction resistance in the isotropic triaxial test was converted into the field condition by multiplying it by 0.67 ( $= (1 + 2K_0)/3$ ). For models 2 and 3, pre-shaking using the input acceleration, which did not cause excess pore pressure ratios greater than 0.5, was repeatedly applied with an ample time interval to fully dissipate any excess pore pressure generated from the preceding events. The pre-shaking was repeated, with the input acceleration amplitude gradually increased, until the target volumetric strain of 0.33% or 0.77% was attained. Destructive shaking was imparted to the model using the estimated input acceleration based on the liquefaction resistance of sand along with the corresponding pre-shearing volumetric strain shown in Fig. 6. Finally, one more shaking event with an input acceleration slightly lower than  $A_0$  was conducted to observe the behavior of sand in re-liquefaction. The choice of the input acceleration for the last event was decided based on the observed results of the triaxial tests [7,23] that once sand experiences liquefaction, its resistance to liquefaction becomes lower than that before the liquefaction.

For models 4 and 5, where wet tamping method was employed as the sand deposition technique to make the sand fabric different, shaking sequences were similar to those of models 1 and 3 but input accelerations were considerably high. This is because the liquefaction resistance of sand deposited by the wet tamping is higher than that deposited by the pluviation method [13]. For model 4, without pre-shaking, the input acceleration amplitude of the first destructive shaking event was 0.75 m/s<sup>2</sup> which was 1.6 times larger than that of model 1. Model 5 was subjected to 12 pre-shakings, which did not cause excess pore pressure ratios greater than 0.35, resulting to a volumetric strain of 1.08%, followed by a destructive shaking with an acceleration amplitude of 1.60 m/s<sup>2</sup>.

#### 4.3. Results and discussions

##### 4.3.1. Models prepared with dry pluviation

Figs. 10 and 11 present histories of maximum input acceleration amplitude, maximum excess pore pressure ratio at the mid-depth of the deposit ( $r_u$ ), and volumetric strain and shear wave velocity throughout the centrifuge experiment for models 1 and 3, respectively.

For model 1, the input acceleration of the first event was 0.5 m/s<sup>2</sup> and was intended to liquefy the sand in the first event so as to observe

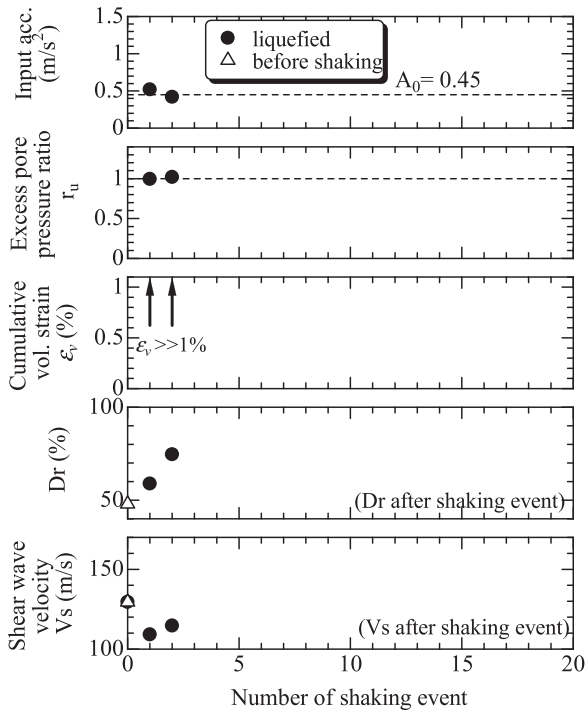


Fig. 10. Sequence of shaking event and responses of model 1.

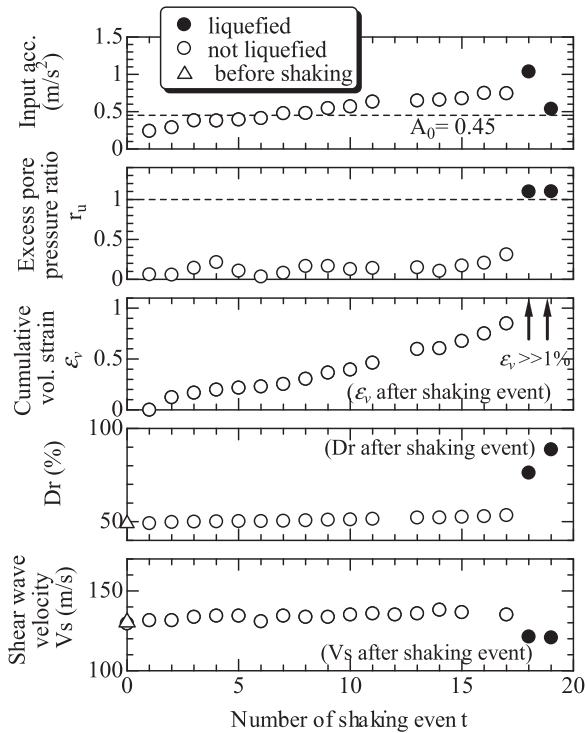


Fig. 11. Sequence of shaking event and responses of model 3.

the liquefaction behavior of the sand without any pre-shaking effects. The model liquefied in several cycles and after shaking, it took about 170–230 s (7–9 s in model scale) to fully dissipate excess pore pressures. A large volumetric strain of 4% and an increase in relative density of 12% were observed. In the second event, the input acceleration amplitude of 0.42 m/s<sup>2</sup>, which was somewhat smaller than A<sub>0</sub>, liquefied the model again. The liquefaction resistance of the sand became smaller after extensive liquefaction, which is consistent with observations in previous studies.

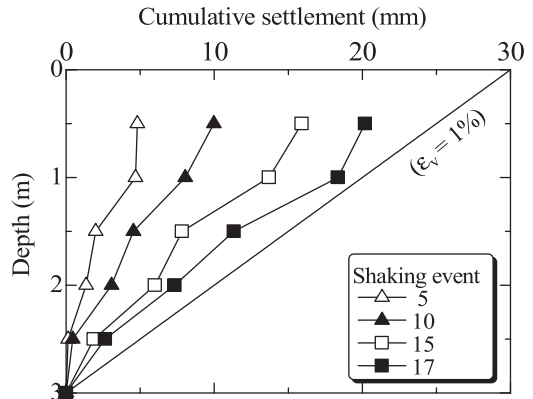


Fig. 12. Evolution of settlement profile with pre-shaking events in model 3.

For model 3, a total of 17 pre-shakings were imparted to the model before destructive shaking tests in the 18th and the 19th events. Fig. 12 indicates the evolution of the settlement profile of the model. Settlement was measured in five depths with potentiometers as shown in Fig. 8. Settlement increased as shaking events continued and at any shaking event is almost linearly distributed, indicating that the volumetric strain of the sand deposit was uniform.

The input accelerations of the first six shaking events were less than A<sub>0</sub> and the generated excess pore pressure ratios were lower than 0.2. In the 7th event, acceleration exceeded A<sub>0</sub> but r<sub>u</sub> was lower than 0.1, clearly suggesting that the pre-shaking history until the 6th event enhanced the sand resistance to pore pressure generation. The input acceleration was increased further with the number of events. When the target volumetric strain of 0.77% was reached after the 17th event, a destructive shaking event was anticipated in the 18th event. The model was shaken at an input acceleration of 1.05 m/s<sup>2</sup>, which was 2.3 times higher than A<sub>0</sub> and as expected, liquefied the sand. In the 19th shaking event, an input acceleration of 0.53 m/s<sup>2</sup> was applied. Interestingly, the sand liquefied again although the input acceleration was approximately half that used in the previous event. The occurrence of extensive liquefaction in the 18th event eliminated the beneficial effects that were acquired through the series of pre-shaking events and the liquefaction resistance of the sand returned to the value equal to or even less than that of the sand before the 1st event. This was quite similar to what was observed by El-Sekelly et al. [5,6] and Goto and Towhata [9], confirming the conclusion reached by Dobry and Abdoun [3].

The relative density of the deposit increased by only 4% by the end of the 17th event; this slight increase does not explain why the deposit survived the 17th event with acceleration approximately two times higher than A<sub>0</sub>. The 18th event caused extensive liquefaction followed by a 20% increase in relative density or 4.2% volumetric strain. This large density change also does not explain the occurrence of re-liquefaction in the 19th event under a smaller input acceleration.

#### 4.3.2. Models prepared with wet tamping

For models 4 and 5 prepared with the wet tamping method, model behavior was quite similar to that of the models prepared with pluviation, except that the input accelerations were higher. Figs. 13 and 14 show histories of input acceleration amplitude, r<sub>u</sub>, volumetric strain, relative density, and shear wave velocity throughout the centrifuge experiment for models 4 and 5, respectively. For model 4, the input acceleration of the first event was 0.75 m/s<sup>2</sup> and was intended to liquefy the sand and observe liquefaction behavior of the sand without pre-shaking effects. In fact, the model did liquefy in several cycles. In the second event, the input acceleration amplitude of 0.45 m/s<sup>2</sup>—which was approximately the same as that of the second shaking of model 1—did not liquefy the sand with an observed maximum excess pore pressure ratio of r<sub>u</sub> = 0.2.

For model 5, input acceleration was gradually increased with the

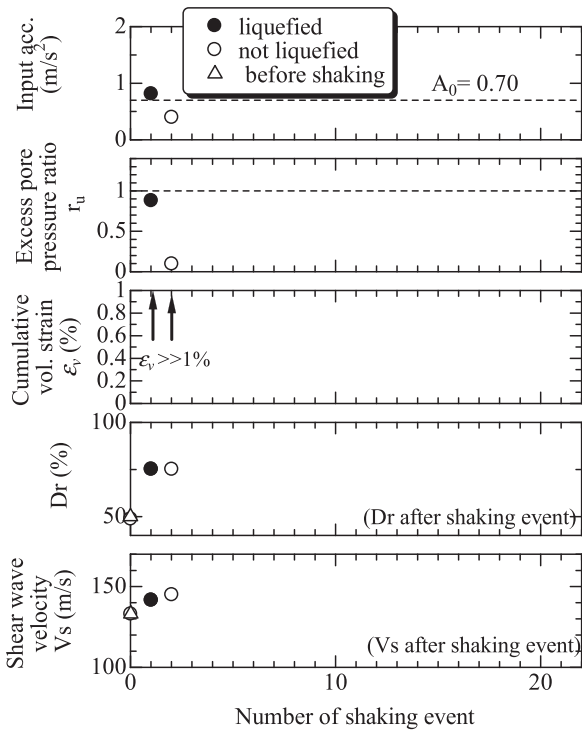


Fig. 13. Sequence of shaking event and model responses of model 4.

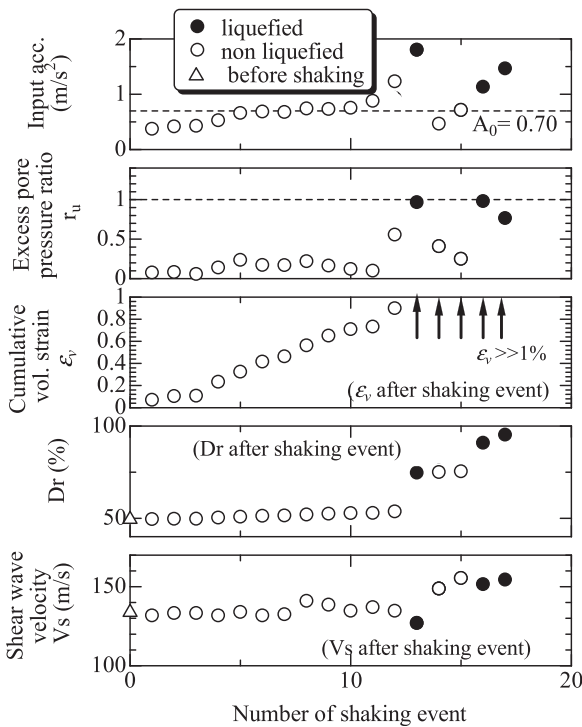


Fig. 14. Sequence of shaking event and model responses of model 5.

number of events and when the target volumetric strain of 0.77% was exceeded after the 12th event, a destructive shaking event was intended in the 13th event. This was achieved by applying an input motion with acceleration amplitude of 1.64 m/s<sup>2</sup>, which liquefied the sand in several cycles. Afterwards, the 14th event was conducted with an input acceleration of 0.50 m/s<sup>2</sup>, which generated an excess pore pressure ratio of  $r_u = 0.7$  but did not cause liquefaction. This observation indicates that the liquefaction resistance of sands with different initial soil fabric, which

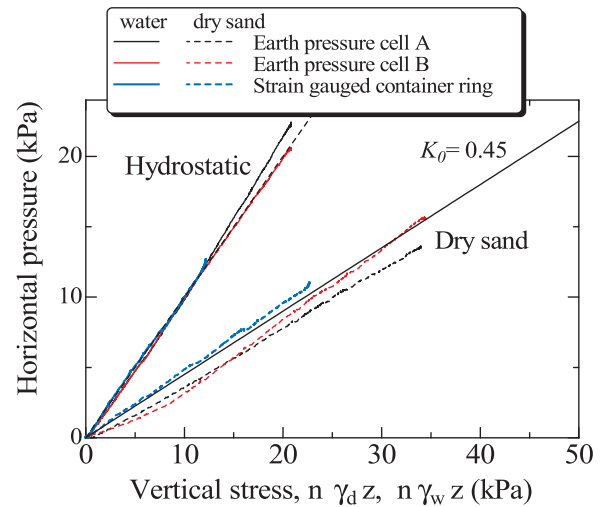


Fig. 15. Calibration results of horizontal earth pressure measurement.

experienced extensive liquefaction, seems to differ.

#### 4.4. Horizontal earth pressure coefficient, $K_0$

Because the liquefaction strength of sand, that is, the cyclic shear stress that can cause liquefaction in a certain number of cycles, is known to be proportional to the mean effective stress [10], the change in the horizontal earth pressures due to pre-shaking is significant in discussing the effects of pre-shaking on the liquefaction resistance. In this study, an attempt was made to measure horizontal earth pressures in two ways.

The rings of the laminar box were designed to behave elastically under the soil and water pressures in the centrifuge environment and the typical strain range of  $0\text{--}2 \times 10^{-2}\%$ . Horizontal pressures on the ring were measured using strain gauges attached to it. Fig. 15 depicts results from calibration tests in which the laminar box was filled with water and hydrostatic pressure increased by increasing centrifugal acceleration. As expected, the strain was practically proportional to the hydrostatic pressure at the depth of the ring and the factor correlating the observed strain with horizontal pressure on the ring was determined. The results of a similar test on dry medium-dense sand ( $\rho_d = 1.51 \text{ g/cm}^3$ ) is also shown in the figure. In the case of dry sand, observed horizontal pressure was also proportional to the vertical pressure at the depth of the ring. Moreover, the coefficient of horizontal pressure at rest,  $K_0$ , within the narrow range of 0.43–0.49, was found to be reasonable.

The other method of measuring earth pressure employed in this study was the use of relatively large earth pressure cells, each 50 mm in diameter and 11 mm thick. The cells were glued to the side wall of the box not to allow different movement from the box. Since dynamic pressures during shaking at different depth are generally not in phase and larger diameter pressure cells are not adequate to measure dynamic pressures. The dynamic component in the measured pressures with the pressure cells are not discussed in this study, but static component after the shaking ceased. As shown in Fig. 15, the pressure cells showed stable performance in the calibration tests. The coefficient  $K_0$  obtained with the cells placed on the sidewall were in the range of 0.40–0.46, which is consistent with those obtained from strains on the ring.

The time histories of horizontal stresses measured by using the earth pressure cell for selected pre-shaking events in model 3 are shown in Fig. 16(a) to (d). The horizontal pressure before the first pre-shaking event was 32 kPa. The horizontal stress in each event increased during shaking—mostly due to the generated excess pore pressure—and then returned to a value slightly higher than that before the shaking (Fig. 16(a), (b), and (c)). By the end of the 17th event, the pressure was

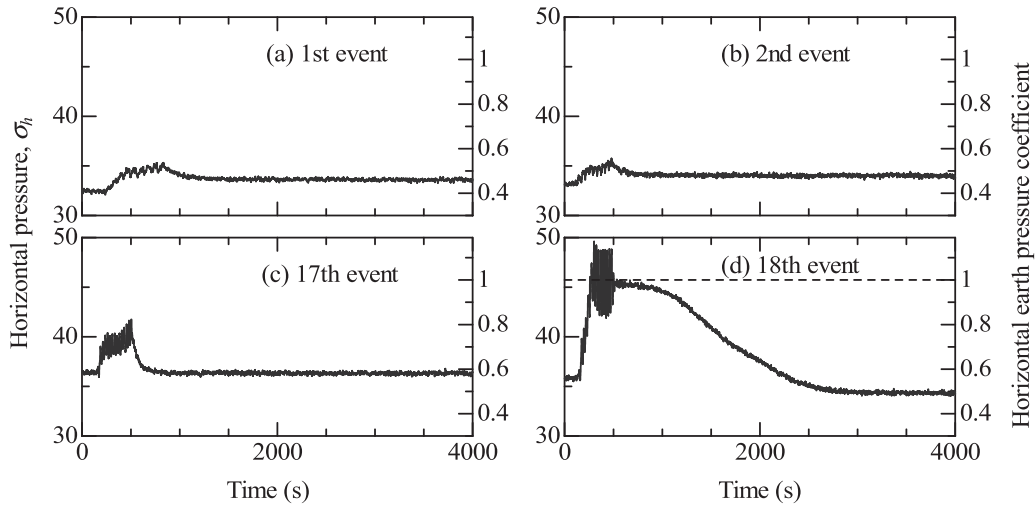


Fig. 16. Time histories of horizontal earth pressure in selected shaking events (model 3).

36 kPa. During the 18th event, when soil liquefied, the measured horizontal pressure reached a value equal to the total overburden pressure of 46 kPa and lasted for 850 s until the excess pore pressure started to dissipate. The pressure after this destructive event settled and stabilized at 33 kPa, which is almost the same pressure before the 1st event.

The values of the coefficient of horizontal pressure at rest,  $K_0$ , in model 3 are chronologically indicated in Fig. 17. At the beginning of the 1st event,  $K_0$  was 0.45, but thereafter, it gradually increased with shaking events and plateaued at 0.57 at the 13th event. Youd and Craven [25] conducted cyclic simple shear test on a dry sand sample, and found that horizontal stress increased with the number of cycles and strain amplitude. At rest, the coefficient of lateral pressure of the sand after 100 cycles of shear, along with about 0.1% strain amplitude, was approximately 0.6. The centrifuge test observations are consistent with that reported by Youd and Craven.

After the dissipation of pore pressure generated during extensive liquefaction in the 18th event,  $K_0$  decreased and returned to a value nearly the same as that before the 1st event. As the pre-shaking proceeded, it was also observed that the earth pressure measured with the cell attached on a box wall perpendicular to the shaking direction becomes larger than that with the cell on a wall parallel to the shaking direction. The same observations are also the case for model 2.

#### 4.5. Shear wave velocity

A pair of bender elements was placed in the model at a depth 2.25 m from the sand surface, as shown in Fig. 8, and used to measure the shear wave velocity ( $V_s$ ) of the sand. Before and after each shaking event, the

sender bender element was excited with one cycle of a sine wave having a frequency of 10 000 Hz and an input voltage of 10 V. The wave that propagated in the soil was recorded by the receiver bender element. The sent wave and the typical output of the received waves are indicated in Fig. 18. The first arrival time of the received wave is identified and the wave velocity was calculated as  $V_s = d/\Delta t$ , where,  $d$  and  $\Delta t$  denote the distance between two bender elements (5 cm tip-to-tip distance in model scale) and the first arrival time, respectively. It should be mentioned that because of the presence of electronic disturbances in the centrifuge, measurements were conducted several times and received signals were stacked to reduce the electronic noise superimposed on the signals.

The shear wave velocities before and after the shaking events are presented in Figs. 10, 11, 13 and 14. Before the first shaking event,  $V_s$  was within a small range of 126–129 m/s for models 1, 2 and 3, and within a range of 133–135 m/s for models 4 and 5. Unless the soil liquefied,  $V_s$  slightly increased with shaking events. For models 2 and 3,  $V_s$  increased by 4 m/s and 9 m/s after the 9th and 17th pre-shaking events, respectively. Once the soil liquefied,  $V_s$  decreased to a value smaller than that before the first shaking event. These observations are quite similar to those reported by Okamura and Hayashi [14].

Fig. 19 depicts the change in shear wave velocity ratio,  $V_s/V_{si}$ , with volumetric strain due to pre-shaking, where  $V_{si}$  stands for the shear wave velocity before the 1st pre-shaking event. Irrespective of the initial grain fabric,  $V_s/V_{si}$  increased with volumetric strain but its increment was smaller than 8% even after the volumetric strain reached 1%. Also shown in the figure are results of the triaxial test on medium-dense Toyoura sand [23]. They prepared specimens with a variety of pre-shearing histories and observed shear wave velocity using

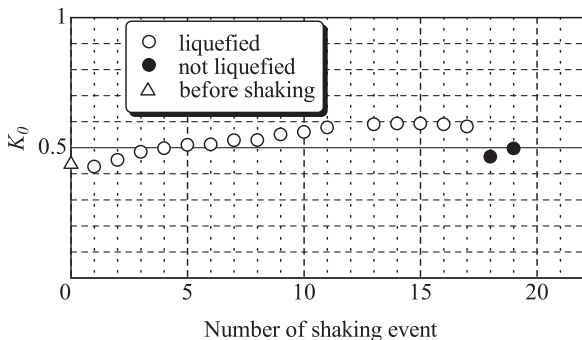


Fig. 17. Evolution of horizontal earth pressure coefficient at the end of each shaking event (model 3).

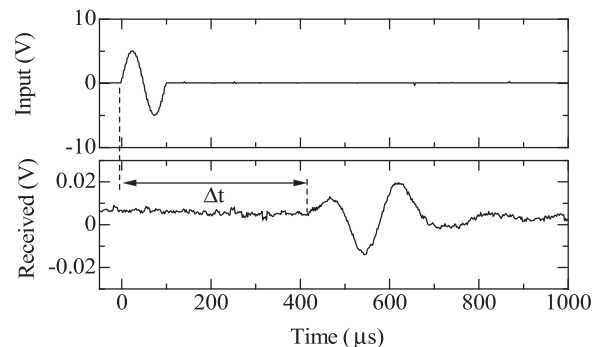


Fig. 18. The sent wave and the typical output of the received waves with bender element placed at depth 2.25 m from the surface of the sand.

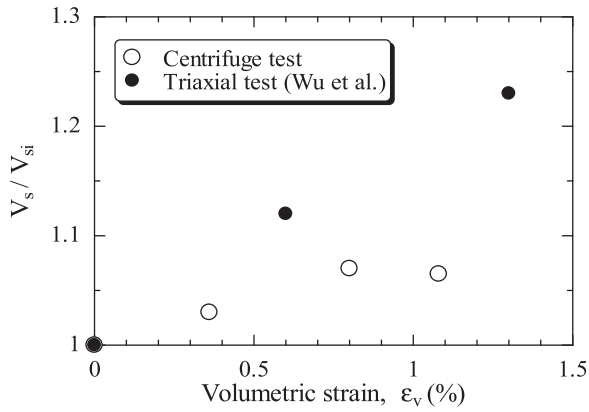


Fig. 19. Relationship between shear wave velocity ratio and volumetric strain due to pre-shakings. The  $V_s$  of Wu et al. [23] was measured in the longitudinal direction of triaxial specimens.

accelerometers attached to the side of the specimens. The source of the shear wave was torsional movement imposed on the cap. The increment in  $V_s/V_{si}$  observed by Wu et al. [23] was significantly higher than the results of the centrifuge tests. Wu et al. [24] also observed shear wave velocity of medium-dense Toyoura sand with and without pre-shearing histories. They put two sets of bender element on the specimens to measure the velocities of shear waves traveling both vertically and horizontally in the specimens. They found that the effects of pre-shearing histories on shear wave velocity depends on the direction the wave traveled. This phenomenon apparently needs further investigation.

#### 4.6. Evaluation of liquefaction resistance

Liquefaction resistance of sand in each model is estimated in this section. Because of the irregular nature of the input acceleration amplitudes and response motions, the method is employed which was proposed by Seed et al. [18] based on cumulative damage hypothesis for metal fatigue evaluations. Shear stress time histories at the middle depth of the models are derived from the acceleration records of the accelerometers a3, a4, and a5, as shown in Fig. 8.

The undrained cyclic triaxial test results on Toyoura sand, with and without pre-shearing, as indicated in Fig. 6, are approximated using linear relationships between the cyclic stress ratio and the number of cycles in log-log plot as,

$$\log(\sigma_d/2\sigma'_c) = R_1 - 0.132 \log(N) \quad (1)$$

where  $R_1$  is the shear stress ratio at  $N = 1$ ,  $\sigma_d/2\sigma'_c$  and  $N$  denote cyclic stress ratio and number of cycles, respectively. Damage by the  $n^{\text{th}}$  half-cycle with a peak cyclic shear stress ( $\tau/\sigma'_v$ ) $_n$  is calculated as,

$$D_n = \frac{1}{2} \left[ \frac{1}{R_1} \left( \frac{\tau}{\sigma'_v} \right)_n \frac{1 + 2K_0}{3} \right]^{0.132}, \quad (2)$$

where,  $\sigma'_v$  is effective vertical stress at the mid-depth of the centrifuge model. The cumulative damage by the time the sand liquefied at the  $N_l^{\text{th}}$  half-cycles is,

$$D_c = \sum_{n=1}^{N_l} D_n \quad (3)$$

When the sand reached the liquefaction condition in the  $N_l^{\text{th}}$  half-cycles, the cumulative damage,  $D_c$ , is equal to unity and  $R_1$  is determined accordingly. Liquefaction resistance,  $R_{L20}$ , which is the cyclic shear stress ratio at  $N = 20$ , is derived from Eq. (1). In view of the fact that the coefficient  $K_0$  observed in the tests was in the small range irrespective of the pre-shaking histories, a value of  $K_0 = 0.5$  is assumed.

The liquefaction resistance ratio,  $LRR$ , obtained from the centrifuge

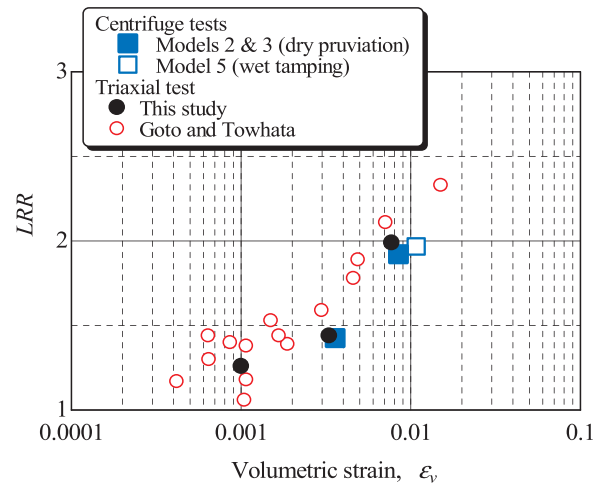


Fig. 20. Relationship between liquefaction resistance ratio and volumetric strain.

tests is shown in Fig. 20. The liquefaction resistance of dry pluviated sands in models 2 and 3 were, respectively, 1.4 times and 1.9 times higher than that in model 1. In addition, the wet tamped sand in model 5 showed 2 times higher resistance to liquefaction than that in model 4. The plots for the centrifuge tests agree quite well with those derived from the triaxial tests.

Note that the coefficient  $K_0$  observed before the pre-shaking was typically 0.46 and that after the pre-shaking events, just before extensive liquefaction, was 0.56 for the heavily shaken model 3. The difference in the mean effective stress ( $(1 + 2K_0)\sigma'_v/3$ ) due to this change in  $K_0$  is only 8%. Nevertheless, the effect of the change in  $K_0$  on the significant increase in the LRR shown in the figure is only marginal.

It is of interest to compare the relationship between the liquefaction resistance of sand and its shear wave velocity with the proposed triggering liquefaction charts, which are extensively used in practice to assess liquefaction potential. The liquefaction assessment charts proposed over the years are calibrated by a number of field case histories of liquefaction and no liquefaction. The data points in the chart include a number of what have been called “false positives,” that is, sites that should have liquefied because they are above the curve, but in fact did not liquefy. In this regard, Fig. 21 indicates results of the centrifuge tests together with a curve for a triggering liquefaction chart proposed by Andrus and Stokoe [1]. Also shown in the figure is a curve proposed by Dobry et al. [4] suitable for recent fills and models which have not experienced any aging effects. The data points corresponding to the pluviated sand without pre-shaking history (model 1) is practically on the curve proposed by Dobry et al. [4]. The data points moved upward almost vertically, rather than moving up along with the proposed curves, and tending to make the data points of sand with pre-shaking history the false positive. This also further confirms the previous finding of Dobry and Abdoun [3] that false positives in the chart are explained by pre-shaking in previous earthquakes. Moreover, it can also be pointed out that initial soil fabric did not affect  $V_s$ . Having considerably different liquefaction resistances, models 1 and 4 showed practically the same  $V_s$ .

## 5. Conclusion

This paper describes the pre-shearing effects on liquefaction resistance both in isotropically confined triaxial testing condition and in one-dimensional free field condition using centrifuge modeling. An attempt was made to explain the effect quantitatively with a single index of the volumetric strain caused by the pre-shearing. The main conclusions obtained from this study are summarized as follows.

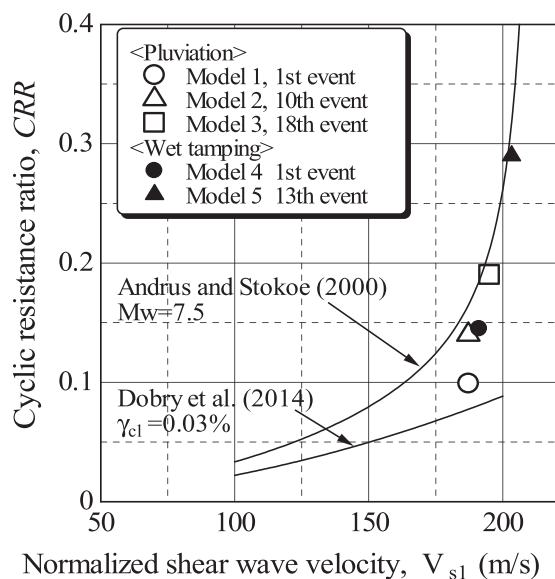


Fig. 21. Relationship between liquefaction resistance ratio and normalized shear wave velocity.

- Through the triaxial tests, it was found that the liquefaction resistance of pre-sheared sand increased with increasing volumetric strain in the pre-shearing process, regardless of the cyclic shear stress ratio and number of cycles in pre-shearing. Based on the test results obtained in this study as well as those found in literature, it is confirmed that there is a unique relationship between the liquefaction resistance ratio—that is, the liquefaction resistance of sand normalized with respect to that of sand without pre-shearing history—and volumetric strain caused by pre-shearing.
- It was reported that liquefaction resistance increases with decreasing degree of saturation and partial drainage during undrained shearing [16]. The volumetric strain that occurs under those conditions has the same effect as that in the pre-shearing. The relationship between LRR and volumetric strain obtained from undrained cyclic triaxial tests on unsaturated sand and from tests on sand at the partially drained condition agrees well with that in the pre-sheared sand. The positive effects of pre-shearing, imperfect saturation, and partial drainage are all uniquely explained in terms of the volumetric strain.
- In the centrifuge tests conducted in this study, the models were subjected to many small shaking events, which were weak enough not to liquefy the model. It was found that the change in index parameters, such as relative density and shear wave velocity, were small and within a few percentage. Hence, relative density and  $V_s$  are poor indicators of the liquefaction resistance of pre-shaken sand.
- The horizontal earth pressures slightly increased as the pre-shaking proceeded but the coefficient  $K_0$  stayed in a relatively small range between 0.48 and 0.57. The difference in the mean effective stress  $((1 + 2K_0)\sigma_v'/3)$  due to this change in  $K_0$  was only 8%. The effect of the change in  $K_0$  on the LRR is only marginal.
- After the pre-shaking events, destructive strong shaking events were imparted to liquefy the models. It was observed that liquefaction resistance was significantly increased by pre-shaking. The relationship between LRR and  $\varepsilon_v$  obtained from the centrifuge tests on models prepared by different methods are well in agreement, suggesting that this relationship is not changed by the initial fabric of the sand. The relationship also compared quite well with that observed in the triaxial tests.
- After extensive liquefaction, all index parameters, excluding soil

density— $K_0$ ,  $V_s$ , and liquefaction resistance — tended to return to their original values before the pre-shakings.

#### Acknowledgements

This study was partly supported by JSPS KAKENHI Grant Number 16H04410.

#### References

- [1] Andrus RD, Stokoe II KH. Liquefaction resistance of soils from shear-wave velocity. *Journal Geotech Geoenviron Eng*, ASCE 2000;126(11):1015–25.
- [2] Andrus RD, Hayati H, Mohanan N. Correcting liquefaction resistance of aged sands using measured to estimated velocity ratio. *J Geotech Geoenviron Eng*, ASCE 2009;135:6:735–44.
- [3] Dobry R, Abdoun T. Cyclic shear strain needed for liquefaction triggering and assessment of overburden pressure factor  $K_0$ . *Journal Geotech Geoenviron Eng*, ASCE 2015;141(11). [04015047-1 to -18].
- [4] Dobry R, Abdoun T, Stokoe II KH, Moss RES, Hatton M, El Ganainy H. Liquefaction potential of recent fills versus natural sands located in high seismicity regions using shear wave velocity. *J Geotech Geoenviron Eng*, ASCE 2014;141(3). [04014112-1 to -13].
- [5] El-Sekelly W, Abdoun T, Dobry R. Liquefaction resistance of a silty sand deposit subjected to preshaking followed by extensive liquefaction. *J Geotech Geoenviron Eng* 2016. [http://dx.doi.org/10.1061/\(ASCE\)GT.1943-5606.000144404015101](http://dx.doi.org/10.1061/(ASCE)GT.1943-5606.000144404015101).
- [6] El-Sekelly W, Dobry R, Abdoun T, Steidl JH. Centrifuge Modeling of the Effect of Preshaking on the Liquefaction Resistance of Silty Sand Deposits. *J Geotech Geoenviron Eng* 2016. [http://dx.doi.org/10.1061/\(ASCE\)GT.1943-5606.00014304016012](http://dx.doi.org/10.1061/(ASCE)GT.1943-5606.00014304016012).
- [7] Finn W, Bransby P, Pickering D. Effect of strain history on liquefaction of sand. *J Soil Mech Found Eng*, ASCE 1970;96(SM6):1917–34.
- [8] Finn W. Liquefaction potential: developments since 1976. In: *Proceedings International Conference Recent Advances in Geotechnical Earthquake Engineering and Soil Dynamics*, 2: 655–681; 1981.
- [9] Goto S, Towhata I. Acceleration of aging effect of drained cyclic pre-shearing and high temperature consolidation on liquefaction resistance of sandy soils. *Geotechnical Eng J*, JGS 2014;9(4):707–19.
- [10] Ishihara K, Iwamoto S, Takatsu H. Liquefaction of anisotropically consolidated sand. *Proc 9th Int Conf Soil Mech Found Eng* 1977;2:261–4.
- [11] Ishihara K, Araki K, Brandley BA. Characteristics of liquefaction-induced damage in the 2011 Great East Japan Earthquake, *Proceedings International Conference Geotechnics for Sustainable Development*, New Zealand; 2011.
- [12] Kiyota T, Koseki J, Sato T, Kuwano R. Aging effects on small strain shear moduli and liquefaction properties of the in situ frozen and reconstituted sandy soils. *Soil Found*, JGS 2009;49(2):259–74.
- [13] Mullilis JP, Seed HB, Chan CK, Michell JK, Arulanandan K. Effect of sample preparation on sand liquefaction. *Journal Geotech Eng Div*, ASCE 1977;103(2):91–108.
- [14] Okamura M, Hayashi S. Damage to river levees by the 2012 Off the Pacific Coast Tohoku Earthquake and prediction of liquefaction in levees, *Geotechnics for Catastrophic Flooding Events*. London: Taylor & Francis Group; 2015. p. 57–67.
- [15] Okamura M, Inoue T. Preparation of fully saturated models for liquefaction study. *Int J Phys Model Geotech* 2012;12(1):39–46.
- [16] Okamura M, Soga Y. Effects of pore compressibility on liquefaction resistance of partially saturated sand. *Soils Found*, JGS 2006;46(5):695–700.
- [17] Seed HB. Soil liquefaction and cyclic mobility evaluation for level ground during earthquakes. *J Geotech Eng Div*, ASCE 1979;105(2):201–55.
- [18] Seed HB, Idriss IM, Makdisi F, Banerjee N. Representation of irregular stress time histories by equivalent uniform stress series in liquefaction analysis, Report No. EERC 75-29, Earthquake Engineering Research Center, Univ. of California, Berkeley; 1975.
- [19] Seed HB, Mori K, Chan CK. Influence of seismic history on liquefaction of sands. *J Geotech Eng Div*, ASCE 1977;103(4):257–70.
- [20] Singh S, Seed HB, Chan CK. Undisturbed sampling of saturated sands by freezing. *J Geotech Eng Div*, ASCE 1982;108(2):247–64.
- [21] Tan TS, Scott RF. Centrifuge scaling considerations for fluid particle systems. *Geotechnique* 1985;35(4):461–70.
- [22] Tokimatsu K, Nakamura K. A Simplified correction for membrane compliance in liquefaction tests. *Soils Found*, JGS 1987;27(4):111–22.
- [23] Wu C, Kiyota T, Katagiri T. Effects of drained and undrained cyclic loading history on small strain shear moduli and liquefaction resistance of medium dense Toyoura sand. *J JSCE A1 (Struct, Geotech Eng)* 2016;72(4):482–8. [in Japanese].
- [24] Wu C, Kiyota T, Katagiri T. Effects of drained and undrained cyclic loading on anisotropy of small strain shear moduli and liquefaction strength of Toyoura Sand. In: *Proc. 51th Japan National Conference on Geotechnical Engineering*; 2016b 1783–1784 (in Japanese).
- [25] Yound TL, Craven TN. Lateral stress in sands during cyclic loading. *J Geotech Eng Div*, ASCE 1975;101(2):217–21.